JOURNAL OF PROPULSION AND POWER
Vol. 26, No. 1, January–February 2010

Theoretical and Experimental Study of the Dynamics of a Liquid Swirl Injector

Qing-fei Fu,* Li-jun Yang,† and Xiang-dong Wang‡
Beijing University of Aeronautics and Astronautics, 100191 Beijing, People's Republic of China

DOI: 10.2514/1.44271

The purpose of this paper is to summarize important aspects of the dynamic characteristic of an open-end swirl injector used in a liquid rocket engine. Theoretical analysis about the dynamic characteristics of open-end swirl injectors has been performed, considering the influence of the axial velocity of liquid in the vortex chamber on the volume flux pulsation. Moreover, the model of interaction between the tangential channel and the vortex chamber has also been modified by taking into account the influence of reflected waves; the formula for the transfer functions of the open-end swirl injectors has been deduced. The dynamics of the open-end swirl injector have been calculated. To investigate the dynamic characteristics of the swirl injector experimentally, an inner flow-pulsation measurement method has been developed according to the characteristics of the liquid flow in the swirl injector. The principle of measuring the instantaneous volume flow using conductance method is discussed. The sensor is composed of a lock-in amplifying circuit and an electronic probe, fabricated from porous titanium material; an experimental measurement of the open-end swirl injector is conducted using this sensor. The experimental result shows that both the method and the sensor can meet the requirement for a flow-pulsation measurement in the swirl injector. This is of considerable significance in the experimental investigation of the swirl injector dynamic characteristics and liquid rocket engine unstable combustion.

Nomenclature

A	=	geometry characteristics parameter
a	=	dimensionless coefficient, $A^2\mu^2 = 2(1-\varphi)^2/(2-\varphi)$
d	=	diameter
K	=	transfer function from the tangential channel to the vortex chamber
Q, q	=	volume flow flux
$\bar{R}_{BX}$	=	R_{BX}/R_c
$\bar{R}_k$	=	closed coefficient, R_K/R_c
r	=	radius
V, v	=	velocity
μ	=	discharge coefficient
ν	=	pulsation damping factor
ξ	=	fluctuation of liquid film
Π	=	transfer function
φ	=	flow area coefficient
Ω	=	surface wave amplitude
ω	=	angular frequency

Subscripts

BX	=	inlet to the vortex chamber
C	=	nozzle
K	=	vortex chamber
$k.c$	=	exit section of the vortex chamber
$k.3$	=	vortex chamber bottom
m	=	air core
T	=	tangential channel
$\sum$	=	summation
ϕ	=	whole injector

Superscripts

-	=	dimensionless parameter
$'$	=	pulsation component

Received 10 March 2009; revision received 9 June 2009; accepted for publication 13 July 2009.

*Ph.D. Student, School of Astronautics.

†Professor, School of Astronautics (Corresponding Author), yangli.jun@buaa.edu.cn.

‡Master Student, School of Astronautics.

I. Introduction

OPEN-END swirl injectors are commonly used in Russian oxidizer-rich staged combustion cycle engines, such as preburner and main chamber injectors used in liquid-oxygen (LOX)/kerosene engines RD-120, RD-170, and RD-180. Figure 1 shows the schematics of a closed and an open-end swirl injector. Compared with the closed swirl injector, there is no nozzle in an open-end swirl injector. In cold-flow conditions, open-end swirl injectors have no advantage in atomization quality compared with closed swirl injectors; in fact, they are less advantageous than the closed swirl injectors. Even so, the open-end swirl injector is still in use because of its good dynamic performance. Because high-thrust liquid-propellant rocket engines have become strong contenders for the next generation of space transportation systems, much more attention has been paid to research on open-end swirl injectors [1].

A great deal of research [2–7] has been done on the dynamic characteristics of the swirl injectors. Acoustic resonance in the vortex chamber and flow damp of LOX to the fluctuation have also been taken into account. The transfer function of a closed swirl injector can be used to calculate the dynamic characteristics of an open-end swirl injector by taking the reflection coefficient to be zero. However, the influence of axial velocity of the liquid at the bottom of the vortex chamber on injector flow pulsation is neglected [2,3]. As there is no convergent nozzle in an open-end swirl injector, it makes the flow mechanism different from that of a closed injector. The difference lies in two factors: First, the axial velocity of liquid flow in the vortex chamber of an open-end swirl injector is greater than that in a closed swirl injector, which has the same vortex chamber diameter. Second, there is no reflected wave in liquid fluctuation process in an open-end swirl injector; the dynamics theory, which ignores the effect of liquid axial velocity in the vortex chamber of an open-end swirl, will cause errors to be made. Zakharov et al. [8] used a boundary element method to study the dynamics of the swirl injectors with multiple rows of tangential inlet channels. The results show that the use of multiple inlet channels is believed to provide a mechanism to cancel waves, and hence injector unsteadiness, at specific frequencies.

Fluctuations of the heat release and acoustic pressure are generated due to the unstable combustion in the combustion chamber. Because there are close relations between the fluctuation of heat release and fluctuation of the injected propellant mass flow rate, it is necessary to investigate the variation of the mass flow rate caused by the pressure fluctuation in the combustion chamber. Variables composing the mass flow rate are the axial velocity and the cross-sectional area. The axial velocity can be acquired from theoretical formulas [2], and the cross-sectional area is measured using an electric conductance method. The fluctuation of the mass flow rate can be acquired through multiplying these two variables. Many studies have been performed using the electric conductance method. Asali and Hanratty [9] measured the interfacial drag and film height for vertical annular flow with electric conductance method. Andreussi et al. [10] used an impedance method to measure the liquid holdup in two-phase flow. Tsochatzidis et al. [11] developed a conductance probe for measuring liquid fraction in pipes and packed beds. More investigations focused on measurement of the liquid-film thickness using the electric conductance method [12–15]. However, these studies mostly focused on the steady states. In recent years, Kim et al. [16,17] performed some experimental research on the dynamic characteristics of a swirl injector; however, most of this experimental research was focused on the closed swirl injector. All of the experiments reported were done in the low-fluctuation frequency range. Yang et al. [18] investigated the spray-field dynamics and droplet-size distribution of a gas–liquid swirl coaxial injector by means of a high-speed photographic technique. The results show that the spray field of the coaxial injector is unsteady and that the sizes of the liquid droplets and the mass flow rate in the spray field are variable.

Theoretical study and numerical simulation of the dynamic characteristics of open-end swirl injectors are examined in this paper. From the result, it can be concluded that the phase lag of an open-end swirl injector linearly increases with the increase of length in the vortex chamber. Therefore, the fluctuation of some frequencies can be filtered by setting the distance between the two rows of tangential channels to an appropriate distance. In fact, open-end swirl injectors used in liquid rocket engine combustion chambers commonly have two rows of tangential channels. Dynamic characteristics of an open-end swirl injector have also been investigated experimentally with an electric conductance method.

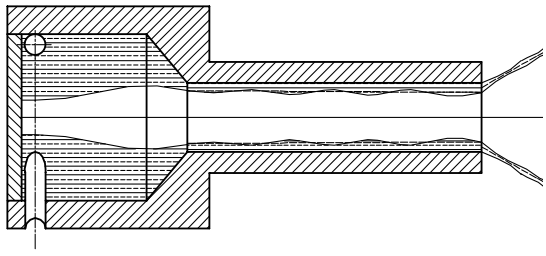

a) Closed swirl injector

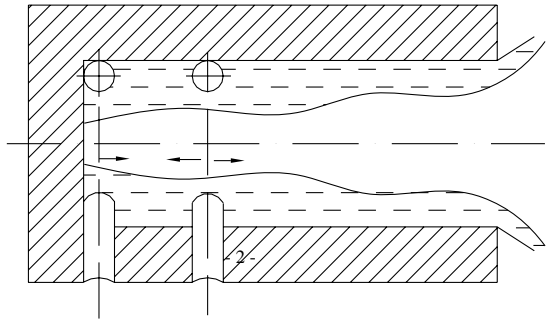

b) Open-end swirl injector

Fig. 1 Schematic of closed and open-end swirl injector.

II. Theoretical Study of Open-End Injector Dynamics

A. Theoretical Formula for the Dynamic Characteristics of an Open-End Swirl Injector

To study its dynamic characteristics, the swirl injector is divided into three components: namely, the tangential channel, the vortex chamber, and the nozzle. This analytical model was used to analyze the closed swirl injector and it was developed by Bazarov [2]. But for an open-end swirl injector, the dynamic characteristics differ greatly from the closed swirl injector, because there is no nozzle in an open-end swirl injector; accordingly, there is no reflected wave propagating along the vortex chamber.

The transfer function of an open-end swirl injector can be defined according to a combination of its parts. For the tangential channel,

$$\prod_T$$

is a complex transfer function of the tangential channel, which denotes the relation of the relative flow pulsation and the relative pulsation of pressure drop in a tangential channel:

$$\frac{Q'_T}{Q_T} = \prod_T \frac{\Delta p'_T}{\Delta p_T} \tag{1}$$

There are two phenomena being considered in the vortex chamber: First, the flow pulsation in tangential channels produces a surface wave in the vortex chamber. Second, the vorticity waves in the fluid regions swirl with different velocities, due to velocity pulsation in the vortex chamber. The vorticity waves strongly depend on the radial velocity in the vortex chamber. The pressure drop in the vortex chamber is the vector sum of the pressure drop due to surface and vorticity waves. $\Pi_{k,3\text{II}}$, $\Pi_{k,3\text{III}}$ are the complex transfer functions of the vortex chamber, which correspond to the two mechanisms of disturbance propagation from the tangential channel to the vortex chamber:

$$\frac{\Delta \mathbf{p}'_{k,3\text{II}}}{\Delta p_T} = \Pi_{k,3\text{II}} \frac{2Q'_T}{Q_T} \tag{2}$$

$$\frac{\Delta \mathbf{p}'_{k,3\text{III}}}{\Delta p_T} = \Pi_{k,3\text{III}} \frac{2Q'_T}{Q_T} \tag{3}$$

When the fluctuation propagates along the vortex chamber, the liquid viscosity can be taken into account by the factor $e^{-\nu\Phi i}$, where ν is the dimensionless pulsation damping factor. If we set the fluctuation of the liquid-film thickness at the bottom of the vortex chamber to be $\xi_{k.3} = \Omega e^{i\omega t}$, the exit section of the vortex chamber will be reached by the surface wave: $\xi_{k.c} = \Omega e^{i\omega(t-t_k)-\nu(\omega t_k)}$, where t_k is the time during which the pulsation propagates from the vortex chamber bottom to the nozzle. If the fluctuation travels one wavelength, the amplitude of the fluctuation will be damped to $1/e^{2\pi\nu}$ times the initial height of the wave, where ν is set to be 0.08 for water at room condition [3]. Therefore, the amplitude of the wave would be damped to 0.6 times the initial height of the wave as it travels one wavelength.

The transfer function for disturbance propagation through the vortex chamber is $\Pi_{k,c\text{II}}$, and the relative flow pulsation at the exit of the vortex chamber is

$$\frac{Q'_{k.c}}{Q_T} = \Pi_{k,c\text{II}} \frac{Q'_T}{Q_T} \tag{4}$$

For a swirl injector, there is always this formula:

$$\Delta \mathbf{p}'_\phi = \Delta \mathbf{p}'_{k,3} + \Delta \mathbf{p}'_T = \Delta \mathbf{p}'_{k,3\text{II}} + \Delta \mathbf{p}'_{k,3\text{III}} + \Delta \mathbf{p}'_T \tag{5}$$

Table 1 Parameters of open-end swirl injectors

Parameters	Values
Diameter of the tangential channel, mm	Φ1.4
Number of tangential channels	3
Length of the tangential channel, mm	5
Diameter of the vortex chamber, mm	Φ5.6, Φ7, Φ7.6, Φ8.4
Length of the vortex chamber, mm	7, 28, 49, 75

For a steady-state injector,

$$\frac{\Delta p_T}{\Delta p_\phi} = \frac{a}{\bar{R}_{BX}^2} \tag{6}$$

Substituting Eqs. (1–4) and (6) into Eq. (5), the total transfer function of the open-end swirl injector can be determined:

$$\Pi_\phi = \frac{Q'_{k.c}}{Q_{k.c}} \Big/ \frac{\Delta p'_\phi}{\Delta p_\phi} = \frac{\bar{R}_{BX}^2}{a} \frac{\Pi_{k,c\text{II}}\Pi_T}{2\Pi_T(\Pi_{k,3\text{II}} + \Pi_{k,3\text{III}}) + 1} \tag{7}$$

A more thorough description is given by Yang and Fu [19]. The characteristics of the transfer function of the open-end swirl injector can be seen in Eq. (7). The total transfer function is complex, and it denotes the relation of relative flow pulsation at the exit of the injector and the relative pulsation of the pressure drop at the injector. Both amplitude and phase can be deduced from this, and it represents the characteristics of an open-end swirl injector in the frequency domain. The component transfer function is also modified because there is no reflected wave in an open-end swirl injector. The coefficient $\bar{R}_{BX}^2/a$ has a minimum value when $\bar{R}_{BX}^2 = 1$, and so the open-end swirl injector has the lowest pulsation amplitude of all types of the swirl injectors. Because of the absence of any reflected waves from the open-end nozzle, there will be no resonance conditions in the vortex chamber. Therefore, there is no transfer function of the nozzle; conditions are greatly simplified.

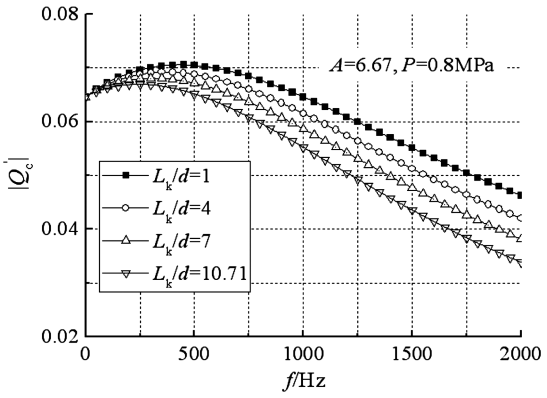

a) Amplitude-frequency diagram

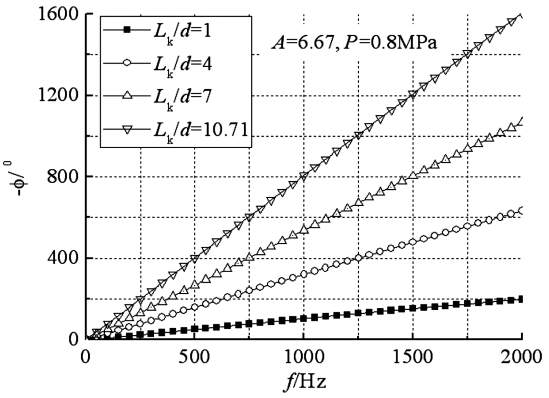

b) Phase-frequency diagram

Fig. 2 Effects of L_k/d on the dynamics of an open-end swirl injector.

B. Influence of Configuration Parameter and Condition Parameter

To study the influence of the injector configuration parameter on the dynamics of an open-end swirl injector, several model injectors were designed to calculate their dynamic characteristics. The parameters of model open-end swirl injectors can be seen in Table 1.

1. *Influence of Ratio of Length/Diameter*

Figure 2 shows the dynamic characteristics of open-end swirl injectors of four different characteristic parameters A and four different ratios of length/diameter, of which $A = 6.67$ and $L_k/d = 10.7$ is the baseline injector in RD-170. It shows that the amplitude of flow pulsation in an open-end swirl injector decreases and the delayed phase increases with the increase of pulsation frequency. When A is given, pulsation amplitude decreases and delayed phase increases as the ratio of length/diameter increases. The vortex chamber is longer; the delayed phase of the vortex chamber is larger because $\Phi_{k.3} = \omega L_k / v_{k.3}$. Because of the existence of liquid viscosity, it can be easily understood when the length of the vortex chamber increases, the damping for the pulsation is much larger, and so the pulsation amplitude is decreased.

2. *Influence of Characteristic Parameter A*

Figure 3 shows the dynamic characteristics of an open-end swirl injector with a different characteristic parameter A. Because

$$A = \frac{R_{BX}R_c}{nR_T^2} = \frac{(Q/n\pi R_T^2) \times \bar{R}_{BX}}{Q/\pi R_c^2} = \frac{\text{tangential velocity} \times \text{arm coefficient}}{\text{axial velocity}} \tag{8}$$

the liquid tangential velocity or arm of force increase as A increases; that is, the moment of momentum increases and the liquid in the swirl injector swirls more intensively.

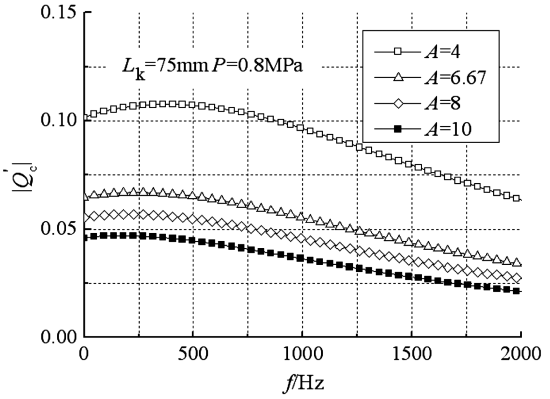

a) Amplitude-frequency diagram

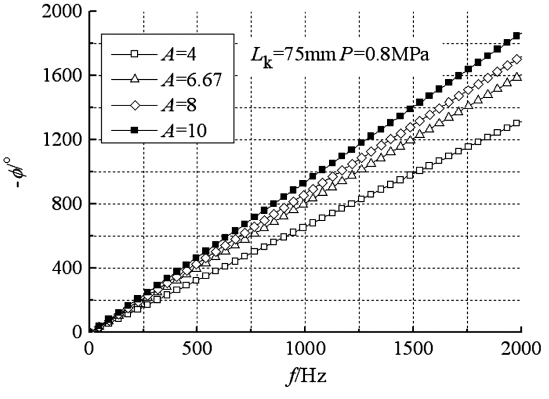

b) Phase-frequency diagram

Fig. 3 Effects of geometrical characteristic A on the dynamics of an open-end swirl injector.

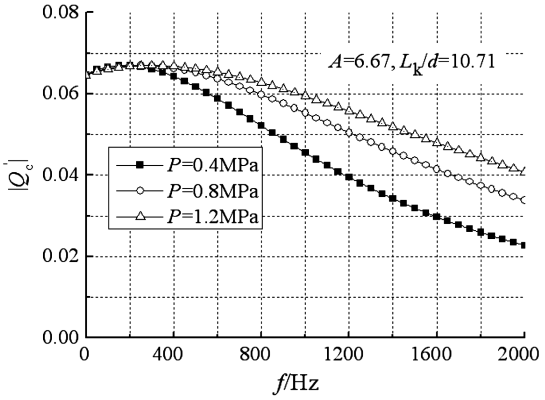

a) Amplitude-frequency diagram

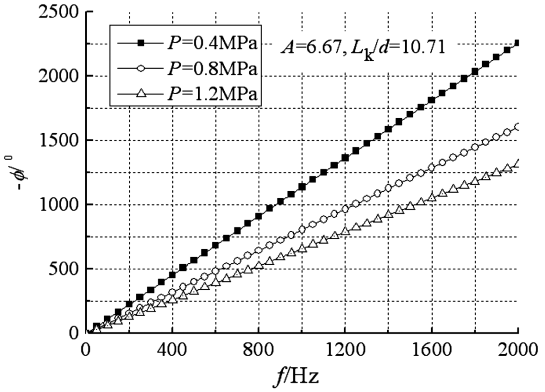

b) Phase-frequency diagram

Fig. 4 Effects of pressure drop on the dynamics of an open-end swirl injector.

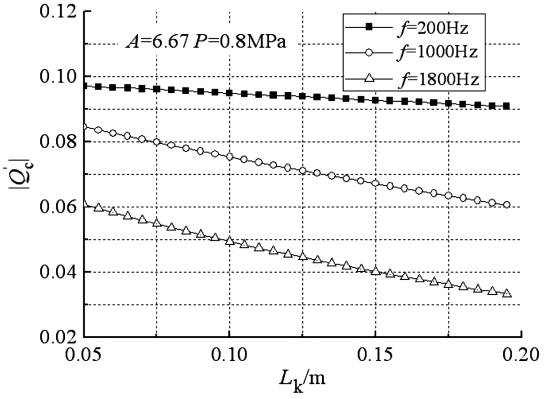

a) Amplitude-frequency diagram

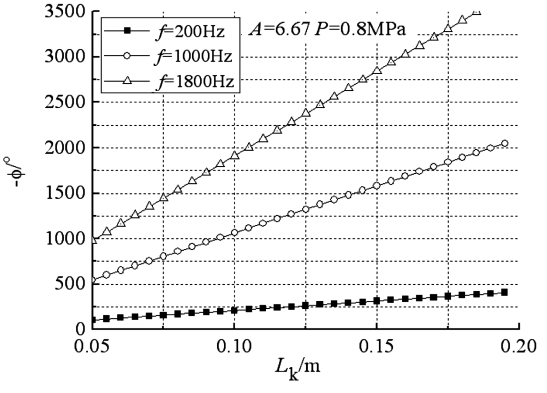

b) Phase-frequency diagram

Fig. 5 Effects of the length of the vortex chamber on the dynamics of an open-end swirl injector.

Figure 3 shows that although the length of the vortex chamber is the same, the amplitude of flow pulsation decreases and the delayed phase increases as A increases; this is because A denotes the swirl strength of liquid flow in the swirl injector. Increased A means that the amplitude of surface wave decreases because of the centrifugal force.

3. Influence of Pressure Drop

Figure 4 shows the dynamic characteristics of an open-end swirl injector under three different pressure drops. For a given open-end swirl injector, the flow pulsation increases and the phase shift decreases when the pressure drop increases; the same is true for the closed swirl injector.

4. Influence of Length of a Vortex Chamber Under Different Fluctuation Frequencies

Figure 5 shows the relation of the dynamic characteristics of an open-end swirl injector via the length of the vortex chamber. The amplitude-frequency diagram shows that the flow-pulsation amplitude at the injector spout decreases, whereas the swirl chamber gets longer; this is because the pulsation would be damped as the length of the swirl chamber increases. The phase shift increases when the vortex chamber length increases, showing the linear growth trend. There is no reflected wave in an open-end swirl injector, and so the phase shift increase is more regular than in a closed swirl injector.

III. Experimental Setup

A. Conductance Measuring Principle

The configuration of the swirl injector is shown in Fig. 6. In the axial direction, define a differential volume dx between cross sections 1-1 and 2-2. It is supposed that the radial coordinates of the surface of the liquid film vary only with the axial coordinate and the time: namely, $r(t, x)$.

At time t_0, the radial coordinate of the liquid-film surface at the axial position x_0 is $r(t_0, x_0)$, and the radial coordinate of the liquid-film surface at $x_0 + \mathrm{d}x$ is

$$r(t_0, x_0 + \mathrm{d}x) \approx r(t_0, x_0) + \frac{\partial r(t, x)}{\partial x}\,\mathrm{d}x \tag{9}$$

The difference of the radial coordinate of the two positions is

$$\Delta = \frac{\partial r(t, x)}{\partial x}\,\mathrm{d}x$$

When $\partial r(t, x)/\partial x$ and dx are minimal, $\Delta \approx 0$. According to experience, the thickness of the liquid film is two orders of magnitude less than the wavelength of the surface wave. Therefore, $\partial r(t, x)/\partial x$ is minor. When dx is minor, it can be supposed that $\Delta \approx 0$, which means that the radial coordinate of liquid film between cross sections 1-1 and 2-2 does not vary with the axial coordinate.

When the liquid is a conductive liquid, the resistance of annular liquid film between cross sections 1-1 and 2-2 can be calculated:

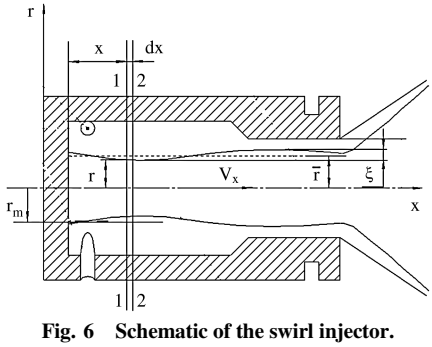

Fig. 6 Schematic of the swirl injector.

$$R_w = \rho_w \frac{\mathrm{d}x}{\pi[R_k^2 - r(t,x)^2]} \tag{10}$$

where R_w is the resistance of the annular liquid film, and ρ_w is the electrical resistivity of liquid.

It can be deduced from Eq. (10) that

$$r(t,x) = \sqrt{R_k^2 - \rho_w \frac{\mathrm{d}x}{\pi R_w}} \tag{11}$$

We suppose the average radius of the liquid film in the spout is $\bar{r}$ and the fluctuation of the liquid-film thickness is $\xi(t,x)$, and so

$$r(t,x) = \bar{r} + \xi(t,x) \tag{12}$$

Substitute Eq. (12) into Eq. (11):

$$\xi(t,x) = \sqrt{R_k^2 - \rho_w \frac{\mathrm{d}x}{\pi R_w}} - \bar{r} \tag{13}$$

It can be seen from Eq. (13) that we can get the fluctuation of liquid-film thickness $\xi(t,x)$ through measuring $R_w(t,x)$ when dx is given.

The relation between the fluctuation of the liquid-film thickness and the instantaneous flow flux is deduced as shown subsequently. A wave equation characterizing the flow oscillation in the liquid film is obtained according to the approach given in [2]:

$$\frac{\partial^2 \xi}{\partial t^2} = \frac{1}{r_m^4} V_{BX}^2 R_{BX}^2 \left(\frac{r^2 - r_m^2}{2}\right) \frac{\partial^2 \xi}{\partial x^2} \tag{14}$$

The surface wave propagation speed

$$C = \frac{V_{BX} R_{BX}}{r_m^2} \sqrt{\frac{r^2 - r_m^2}{2}} \tag{15}$$

The expression for the wave speed is analogous to that for shallow-water wave propagation. The solution to Eq. (14) for a semi-infinite vortex is

$$\xi = \xi_{\max} e^{i\omega(t - x/C)} \tag{16}$$

where $\xi_{\max}$ represents the maximum amplitude of the liquid-surface wave. For an axisymmetric rotating flow with a free interior surface, linearization of equations of motion leads to a relationship between the fluctuation of the liquid surface and axial velocity:

$$\frac{\partial V_x'}{\partial t} = \frac{V_{BX}^2 R_{BX}^2}{r_m^3} \frac{\partial \xi}{\partial x} \tag{17}$$

The integral of the Eq. (17) is

$$V_x' = \frac{V_{BX}^2 R_{BX}^2}{C r_m^3} \xi = \frac{V_{BX}^2 R_{BX}^2}{C r_m^3} \xi_{\max} e^{i\omega(t - x/C)} \tag{18}$$

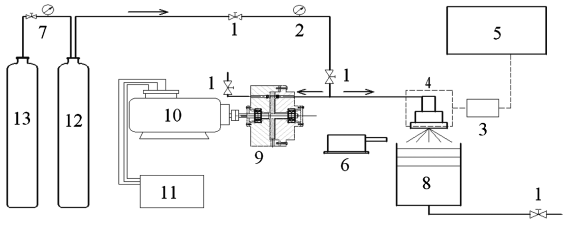

1–regulator valve; 2–pressure gauge; 3–measurement circuit; 4–injector; 5–computer; 6–video camera; 7–relief valve; 8–collector; 9–pulsing flow generator; 10–motor; 11–converter; 12–high pressure water tank; 13–high pressure gas tank

Fig. 7 Schematic diagram of the experimental system.

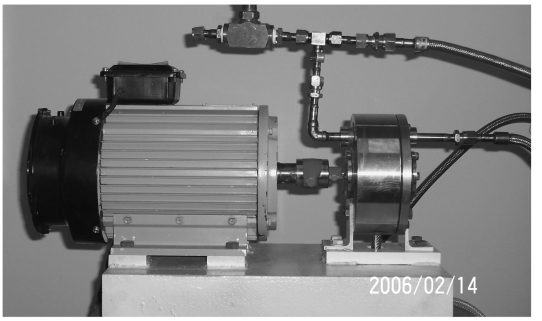

Fig. 8 Schematic diagram of the flow-pulsation generator.

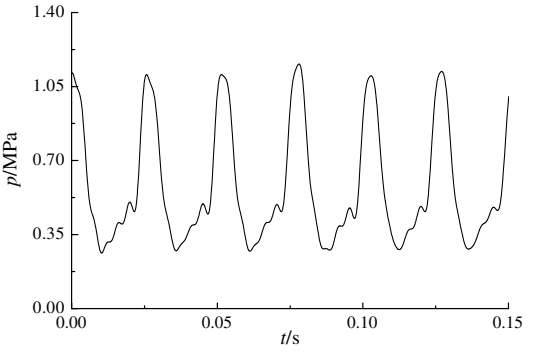

Fig. 9 Pressure signal generated by flow pulse generator.

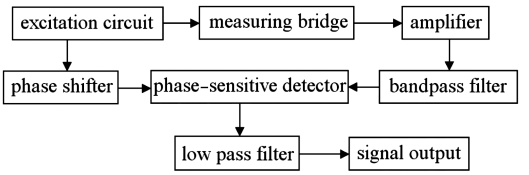

Fig. 10 Schematic diagram of the flow measuring circuit.

The amplitude of the axial velocity fluctuation is

$$|V_{x\max}'| = \xi_{\max} V_{BX}^2 R_{BX}^2 / (C r_m^3) \tag{19}$$

It can be seen from Eq. (18) that the phase of the axial velocity fluctuation and the liquid-film-thickness fluctuation is the same.

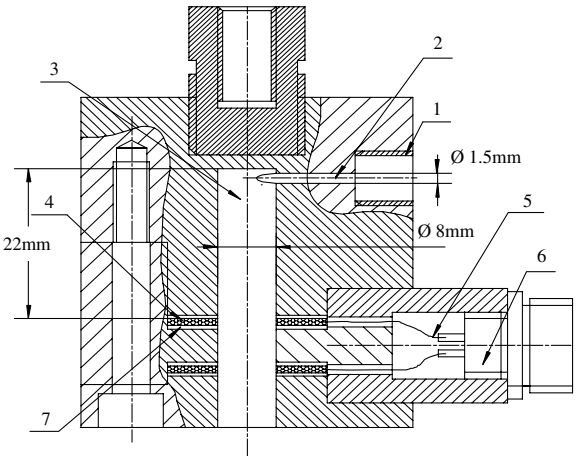

1–inlet of injector; 2–tangential channel; 3–swirl chamber; 4–measuring probe; 5–wire; 6–junction; 7–gasket

Fig. 11 Schematic diagram of the model injector.

Table 2 Configuration parameters of a model injector

Parameters	Values
R_T, mm	0.75
Distance of probes, mm	4
R_{BX}, mm	4
R_C, mm	4

The instantaneous flow can be written in

$$q = \bar{q} + q' = 2\pi \int_{r_m-\xi}^{R_k} (V_x + V_x')r\,\mathrm{d}r \tag{20}$$

Integrate Eq. (20) and neglect the small part of high order, then substitute Eq. (17), and we can get

$$q = 2\pi V_x(R_k^2 - r_m^2) + 2\pi V_x r_m \xi + \pi \frac{V_{BX}^2 R_{BX}^2}{C r_m^3}\xi(R_k^2 - r_m^2) \tag{21}$$

Substitute Eq. (13) into Eq. (21):

$$q = 2\pi V_x(r_k^2 - r_m^2) + 2\pi V_x r_m\left[\sqrt{R_k^2 - \rho_w \frac{\mathrm{d}x}{\pi R_w}} - \bar{r}\right] + \pi \frac{V_{\mathrm{in}}^2 r_{\mathrm{in}}^2}{C r_m^3}\left[\sqrt{R_k^2 - \rho_w \frac{\mathrm{d}x}{\pi R_w}} - \bar{r}\right](r_k^2 - r_m^2) \tag{22}$$

Because the phase of the axial velocity fluctuation and liquid-film-thickness fluctuation is the same, the instantaneous volume flow of the swirl injector can be obtained through Eq. (22). The steady axial velocity is

$$V_x = \frac{\bar{q}}{\pi(R_k^2 - r_m^2)} \tag{23}$$

The instantaneous volume flow can be expressed by the instantaneous resistance of the annular liquid film.

B. Experimental System

To validate the theory of the dynamics of an open-end swirl injector, a series of experiments has been performed. The schematic of the experimental system is shown in Fig. 7. The experimental system is composed of a flow-pulsation-generating system, a dynamic pressure and flow measurement system, a data acquisition system, and a water collector system. To remove the influence of pipeline vibration, a pressurized-water supply system is adopted. High-pressure gas forces water flowing through the regulator valve to the injector. The flow-pulsation generator 9 on the branch pipe generates flow pulsation, which propagates to the injector. The frequency of flow pulsation can be regulated using a frequency converter. The flow-pulsation amplitude can be adjusted by changing the jaw opening of the regulator valve. The response frequency of the pressure sensor is 0–100 KHz, the measuring range is 0–1.5 MPa, and the precision is 0.15%.

The flow-pulsation generator is the most important component in the experimental system. The flow-pulsation generator is powered by a motor delivered by a shaft; the rotary table rotates at high speed. The holes on the rotary table connect to the flow pipe in some predetermined period, and so the flow fluctuates at a certain frequency. Figure 8 demonstrates a schematic of the flow-pulsation generator. Figure 9 is the pressure signal generated at some frequency.

Flow pulsation can be attained by measuring the thickness of the liquid film [2]. The thickness of the liquid film can be found by measuring its conductance. A detailed method uses two porous titanium rings as probes, fixed in the vortex chamber of the injector. When the pulsation flow enters the vortex chamber through the tangential channel, a pulsing liquid film will appear on the vortex chamber wall. The conductance between the two probes varies, and the variation of conductance will be processed by succeeding measuring circuit; thus, the signal relative to flow pulsation will be determined.

The measuring circuit is designed into the lock-in amplifier structure, which is widely used to detect weak signals because of its ability to suppress noise. The pulsation of liquid film is very small and always accompanied by considerable noise, and so the lock-in amplifier is very appropriate for measuring. The detailed structure of the measuring circuit is shown by Fig. 10.

The model injector is shown in Fig. 11. To maintain the insulation of the probes, the injector is made of Lucite. A terafluoroethylene gasket maintains the insulation of the probe and injector. The distance between two probes should be much less than the wavelength of the surface wave in the swirl injector. We suppose that the frequency of the surface wave is 1000 Hz, and the speed of the surface wave can be calculated by Eq. (15); therefore, the wavelength of the surface wave is approximately 22 mm, which is much larger than the distance between two probes. The detailed configuration parameter is shown in Table 2.

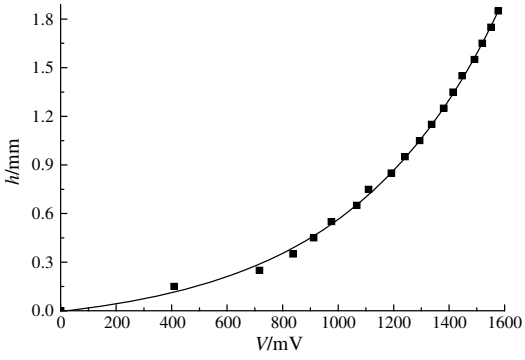

Fig. 13 Calibration curve.

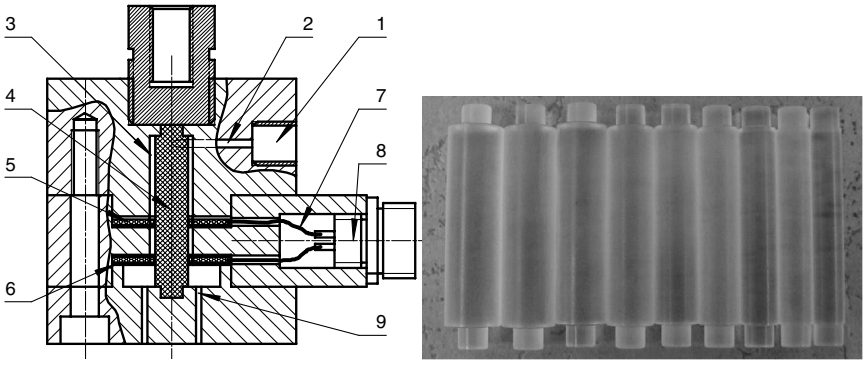

1.front cavity, 2.tangential channel, 3.annular passage, 4.perspex post, 5.probe, 6.gasket, 7.probe wire, 8.junction, 9.effusion passage

Fig. 12 Schematic of the calibration device.

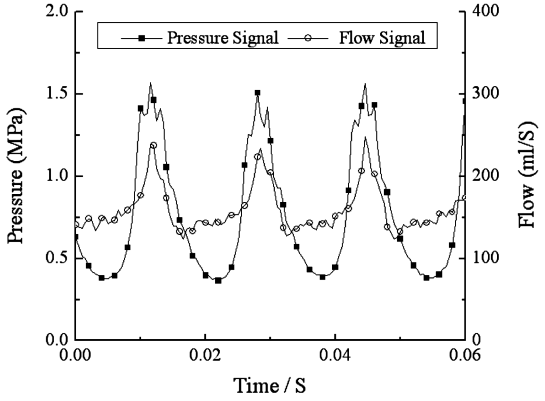

a) Frequency=60 Hz

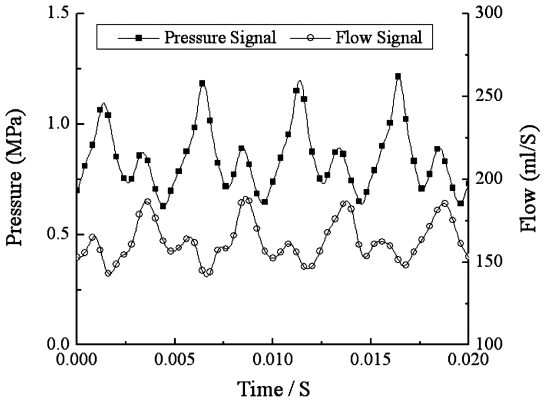

b) Frequency=200 Hz

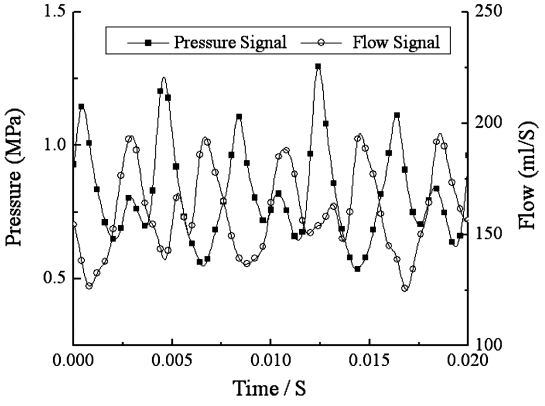

c) Frequency=250 Hz

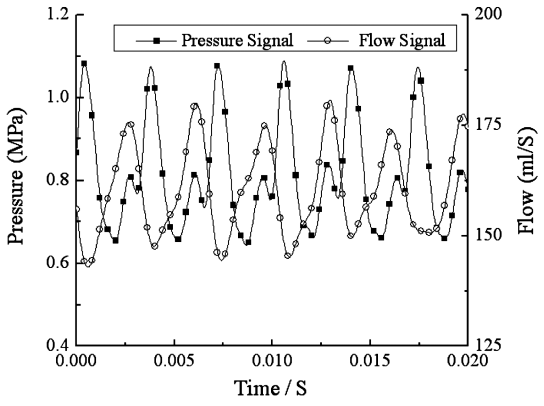

d) Frequency=300 Hz

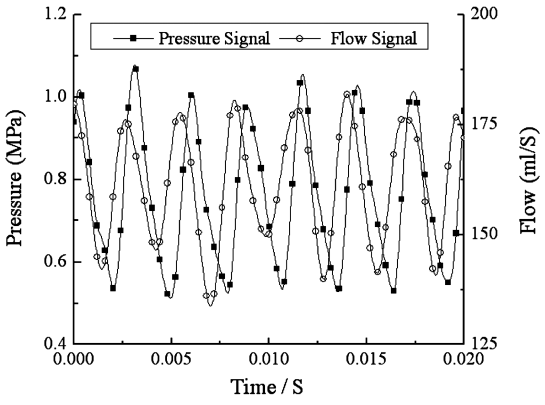

e) Frequency=350 Hz

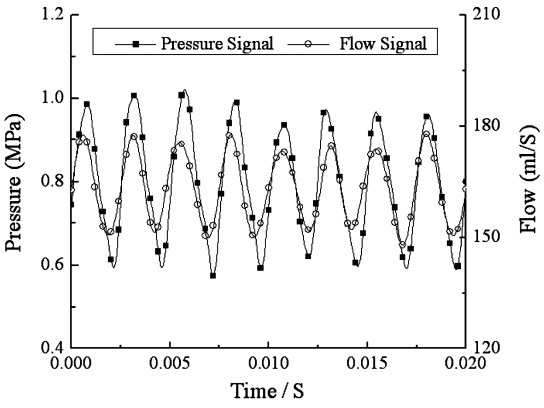

f) Frequency=400 Hz

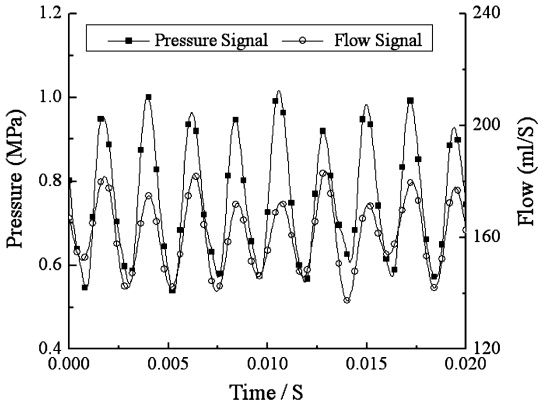

e) Frequency=450 Hz

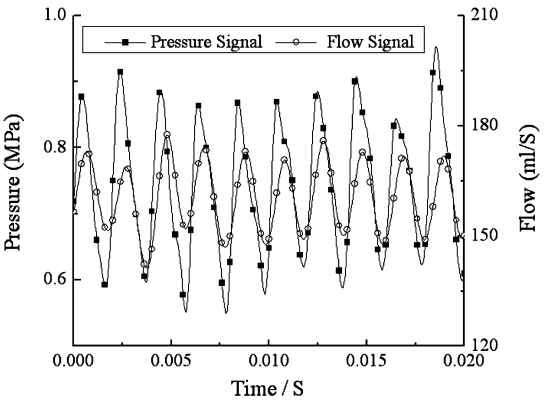

f) Frequency=500 Hz

Fig. 14 Pressure and flow-pulsation signals under different frequencies.

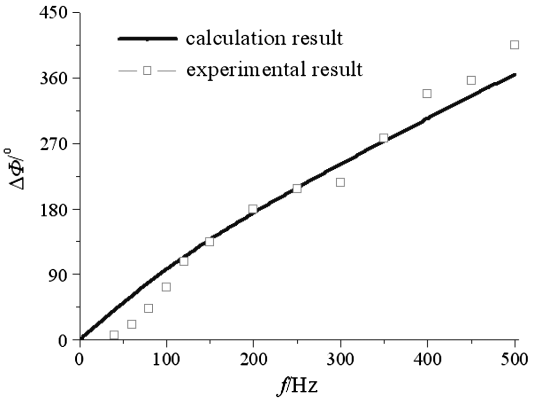

Fig. 15 Contrast of calculation and experimental results.

The sensor is calibrated by measuring the resistance of the standard liquid film that is formed in a fabricated calibration device. The calibration device is shown in Fig. 12. A series of Perspex posts with different diameters correspond to different liquid-film thicknesses. The Perspex posts are fabricated with a tolerance of 0.01 mm. The calibration results are shown in Fig. 13.

C. Experimental Process and Results

To validate the theory of the dynamics of the open-end swirl injector, a series of experiments has been done with the model injectors. The flow pulsation in the vortex chamber and the pressure-pulsation signal are measured under different pulsation frequencies. The phase lag between the two signals is calculated.

Figure 14 shows flow-pulsation and pressure-pulsation signals in the model injector under different pulsation frequencies. In Fig. 14 we can see the pressure and the instantaneous flow fluctuate at the given frequency. The phase lags of the two signals are different under different fluctuation frequencies, which we call the phase-frequency characteristics of the open-end swirl injector.

The phase lag at the wave crest of the two signals is calculated, and contrast with calculation results is noted. The contrast results are shown in Fig. 15.

It shows in Fig. 15 that the experimental result agrees well with the calculation result. The phase lag between the pressure oscillation and the flow oscillation increases when the fluctuation frequency increases, both in the calculation result and the experimental result. The open-end swirl injector dynamics theory is partially verified by the experimental results.

IV. Conclusions

Calculation results show that the amplitude of relative flow pulsation in an open-end swirl injector decreases and the delay phase increases with the increase of the pulsation frequency. The flow-pulsation amplitude increases and the phase shift decreases when pressure drop increases. This condition reverses by increasing A. The flow pulsation decreases and the phase shift increases when parameter A increases. When A is given, flow pulsation decreases and the delay phase increases when the vortex chamber length increases. The result shows that an injector with large geometric characteristics parameter A and a long vortex chamber can damp more flow pulsation.

The experiment is an important part of injector dynamics study. The principle of measuring the instantaneous flow using the conductance method is discussed. The flow-pulsation generator is the most important component of an injector dynamics experimental system. The pulsation signal is poor at lower frequencies, and so the flow-pulsation generator must be improved. The measuring circuit is designed into the lock-in amplifier structure. This type of circuit is widely used to detect liquid conductance because of its ability to suppress noise. The experimental and calculation results agree well, and theory of the open-end swirl injector dynamics is verified.

Acknowledgment

The financial support of China National Nature Science Funds (support number 50406007) is gratefully acknowledged.

References

[1] Dranovsky, M., *Combustion Instabilities in Liquid Rocket Engines: Testing and Development Practices in Russia*, edited by V. Yang, F. E. C. Culick, and D. G. Talley, Progress in Astronautics and Aeronautics, Vol. 221, AIAA, Reston, VA, 2007, p. 320.

[2] Bazarov, V., *Dynamics of Liquid Injectors*, Mashinostroenie, Moscow, 1979.

[3] Bazarov, V., and Yang, V., "Liquid-Propellant Rocket Engine Injector Dynamics," *Journal of Propulsion and Power*, Vol. 14, No. 5, Sept.–Oct. 1998, pp. 797–806. doi:10.2514/2.5343

[4] Bazarov, V., "Influence of Propellant Injector Stationary and Dynamic Parameters on High Frequency Combustion Stability," AIAA Paper 96-3119, 1996.

[5] Balasubramanyam, M. S., Chen, C. P., and Bazarov, V., "Numerical Design Investigation of a Hydro-Mechanical Pulsator for Liquid Rocker Injector Research," AIAA Paper 2008-5230, 2008.

[6] Cavitt, R. C., Frederick, R. A., Jr., and Bazarov, V., "Experimental Methodology for Measuring Combustion and Injection-Coupled Responses," AIAA Paper 2006-4527, 2006.

[7] Bazarov, V., Yang, V., and Puri, P., "Dynamics of Liquid Rocket Injectors," *Liquid Rocket Thrust Chambers: Aspects of Modeling, Analysis, and Design*, Progress in Astronautics and Aeronautics, Vol. 200, AIAA, Reston, VA, 2004, pp. 19–103.

[8] Zakharov, S. I., Richardson, R., and Heister, S. D., "Hydrodynamic Modeling of Swirl Injectors with Multiple Rows of Tangential Channels," AIAA Paper 2006-5202, 2006.

[9] Asali, J. C., and Hanratty, T. J., "Interfacial Drag and Film Height for Vertical Annular Flow," *AIChE Journal*, Vol. 31, No. 6, 1985, pp. 895–902. doi:10.1002/aic.690310604

[10] Andreussi, P., Di Donfrancesco, A., and Messia, M., "An Impedance Method for the Measurement of Liquid Hold-Up in Two-Phase Flow," *International Journal of Multiphase Flow*, Vol. 14, No. 6, 1988, pp. 777–785. doi:10.1016/0301-9322(88)90074-2

[11] Tsochatzidis, N. A., Karapantsios, T. D., Kostoglou, M. V., and Karabelas, A. J., "A Conductance Probe for Measuring Liquid Fraction in Pipes and Packed Beds," *International Journal of Multiphase Flow*, Vol. 18, No. 5, 1992, pp. 653–667. doi:10.1016/0301-9322(92)90037-H

[12] Coney, M. W. E., "The Theory and Application of Conductance Probes for the Measurement of Liquid Film Thickness in Two-Phase Flow," *Journal of Physics E: Scientific Instruments*, Vol. 6, No. 9, 1973, pp. 903–910. doi:10.1088/0022-3735/6/9/030

[13] Gu, D., and Zhu, J., "A Technique for Measuring Dynamic Liquid Film Thickness," *Journal of Chemical Industry and Engineering (China)*, No. 3, 1988, pp. 374–378.

[14] Hu, Z., and Wang, Y., *Engineering Electrical Conductivity Measurement Technology*, Tianjin Univ. Press, Tianjin, PRC, 1990.

[15] Liu, T., and Huang, Z., "Two New Measurement Techniques of Liquid Conductivity," *Control and Instruments in Chemical Industry (China)*, Vol. 32, No. 3, 2005, pp. 50–53.

[16] Kim, D., Im, J. H., Koh, H., and Yoon, Y., "Effect of Ambient Gas Density on Spray Characteristics of Swirling Liquid Sheets," *Journal of Propulsion and Power*, Vol. 23, No. 3, 2007, pp. 603–611. doi:10.2514/1.20161

[17] Kim, S., Kim, D., Khil, T., and Yoon, Y., "Effect of Geometry on the Liquid Film Thickness and Formation of Air Core in a Swirl Injector," AIAA Paper 2007-5460, 2007.

[18] Yang, L., Ge, M., Zhang, M., Fu, Q., and Cai, G., "Spray Characteristics of a Recessed Gas-Liquid Coaxial Swirl Injector," *Journal of Propulsion and Power*, Vol. 24, No. 6, 2008, pp. 1332–1339. doi:10.2514/1.23977

[19] Yang, L., and Fu, Q., "Theoretical Study of Dynamic Characteristic of Open-End Liquid Swirl Injector," International Astronautics Conference, Paper IAC-06-C4.P.309, 2006.

D. Talley
Associate Editor